CORRECTION AND SCOPE

From U(1) to U(N) and a Helicity-2 Sector in a Shared Square-Root-Ladder Register Architecture

The shared register implements a link algebra. Its linear helicity-2 response uses a separate construction. Coexistence of both phases in one microscopic Hamiltonian remains open.

Manuscript · p. 1, abstract

Spin-2 search · null result

Evidence · QATNU/SRQID dated scientific review / One-Hamiltonian composition requirements

From $U(1)$ to $U(N)$ and a Helicity-2 Sector in a Shared Square-Root-Ladder Register Architecture

Joshua Farrow[1]

[1] *Independent Research*

(Dated: June 20, 2026)

We test how far a square-root edge-register architecture can be extended beyond an Abelian quantum link and whether the same local register algebra can support a controlled linear helicity-2 sector. Two color-resolved banks of square-root ladders at fixed total rishon number realize the exact finite-dimensional $U(N_c)$ quantum-link algebra. We audit $N_c = 2, 3, 4$, exact non-Abelian matter hopping, $SU(2)$ and $SU(3)$ Wilson loops, and a mobile two-color controller that generates the matrix Wilson holonomy at fourth order while commuting with every local non-Abelian Gauss generator. Gauge-breaking leakage is suppressed as $\Lambda^{-2.00019}$. A nontrivial obstruction appears: for commuting bosonic rishons, $\det U$ vanishes identically with one flavor. Adding at least N_c flavors makes the determinant nonzero, exactly $SU(N_c)$ invariant, and charged under the extra link $U(1)$, thereby supplying a controlled route from $U(N_c)$ to $SU(N_c)$.

For the tensor branch, six symmetric spatial components are reduced by transverse-traceless constraints. Across 500 random lattice momenta, the physical projector has rank exactly two, Ward residuals below 1.5×10^{-15}, and the rotation character $2\cos 2\theta$ to 6.7×10^{-16}. The lattice gap scales as $L^{-0.999545}$, the tensor susceptibility as $L^{1.999090}$, and cubic anisotropy as $a^{1.99929}$. Square-root ladders reproduce the multiparticle tensor-oscillator spectrum to 10^{-14}, whereas unit-amplitude ladders fail at order unity. Finally, a specified Friedrichs reduction of a gapped three-dimensional pair continuum yields a unique isolated dressed tensor pole below threshold and a broadened response after continuum entry. These results construct controlled non-Abelian and linear helicity-2 sectors in an extended register architecture. They do not show that the original minimal QATNU Hamiltonian inevitably generates a non-Abelian gauge group, electromagnetism, or nonlinear gravity.

I. STATUS AND MOTIVATION

Finite-dimensional quantum links replace Wilson link variables by operators in a finite Hilbert space while retaining an exact local gauge transformation law [1, 3]. Rishon representations make this algebra explicit through bilinears of local constituent modes [2]. The earlier paired-ladder construction established that two square-root ladders can host an exact $U(1)$ quantum link. The first question here is whether the same register logic extends to non-Abelian color.

The second question comes from a separate tensor investigation. Independent static and dynamical probes showed that uncoupled edge ladders do not generate a collective tensor critical mode. Direct inter-edge bilinears can produce propagating tensor-shaped oscillators, but diagonal traceless combinations alone do not establish a helicity-2 gauge sector. A proper linear spin-2 construction requires all six symmetric spatial components, exactly two physical transverse-traceless (TT) polarizations, the helicity-2 rotation law, controlled source decoupling, and a matter-coupled pole rather than a bare-threshold slogan. Related spin models have shown that helicity-2 modes can arise only when an appropriate linearized gauge redundancy is present [4].

This report therefore pursues one shared-register program:

$$\begin{aligned} &\text{square-root ladders} \longrightarrow U(N_c) \text{ quantum links,} \\ &\text{square-root ladders} \longrightarrow \text{a gauge-fixed linear TT sector.} \end{aligned} \tag{1}$$

The result is constructive. The required color multiplicity, flavor extension, fixed-number sectors, TT constraints, and direct couplings are stated explicitly rather than claimed to emerge automatically.

II. COLORED PAIRED LADDERS AND EXACT $U(N_c)$

A. One-link construction

Give every oriented link two banks of bosonic square-root ladders,

$$a_{\alpha f}, \quad b_{\alpha f}, \qquad \alpha = 1, \ldots, N_c, \qquad f = 1, \ldots, N_f, \tag{2}$$

where α is color and f is an optional flavor. Select a fixed total rishon number

$$\mathcal{N} = \sum_{\alpha f} \left(a^\dagger_{\alpha f} a_{\alpha f} + b^\dagger_{\alpha f} b_{\alpha f} \right). \tag{3}$$

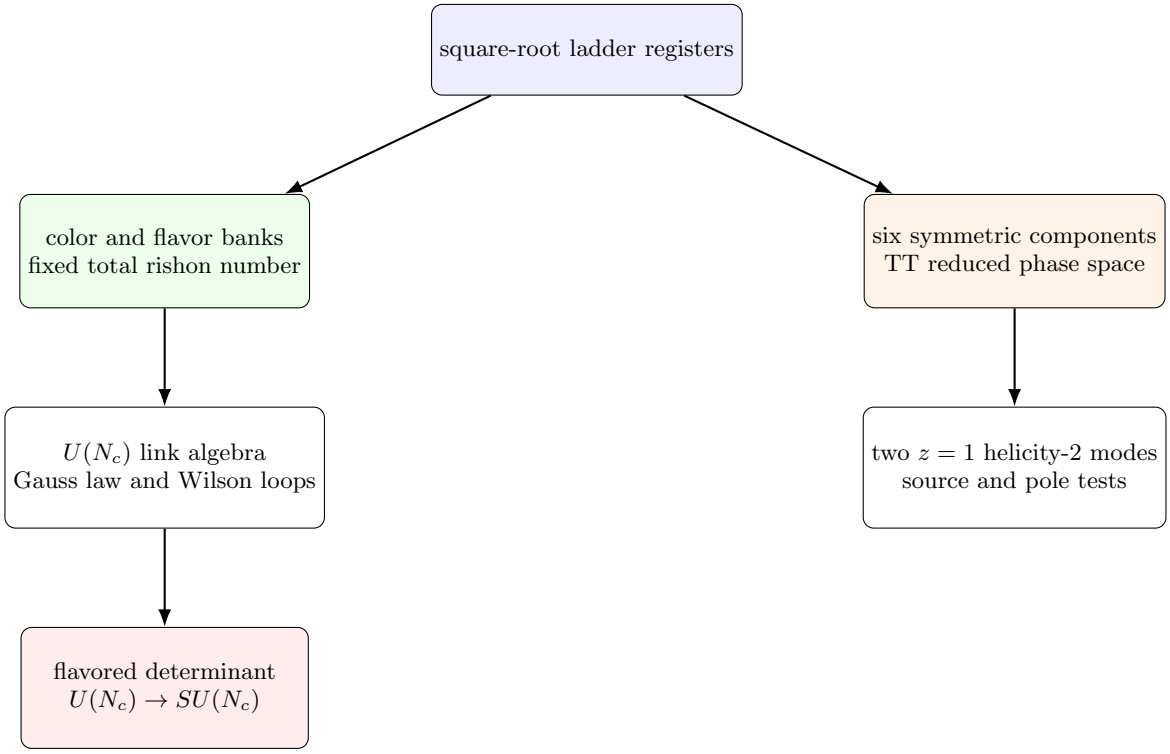

FIG. 1. Scope of the shared-register extension. The non-Abelian and tensor sectors use the same square-root ladder algebra in different controlled sectors. None of the indicated constraints or added multiplicities is hidden.

For fundamental generators T^A normalized by $\mathrm{Tr}\, T^A T^B = \delta^{AB}/2$, define

$$L^A = \sum_{\alpha\beta f} a^\dagger_{\alpha f} T^A_{\alpha\beta} a_{\beta f}, \tag{4}$$

$$R^A = \sum_{\alpha\beta f} b^\dagger_{\alpha f} T^A_{\alpha\beta} b_{\beta f}, \tag{5}$$

$$U_{\alpha\beta} = \sum_f a_{\alpha f} b^\dagger_{\beta f}, \tag{6}$$

$$E = \frac{1}{2}(N_R - N_L). \tag{7}$$

Our orientation convention gives

$$[L^A, L^B] = \mathrm{i} f^{ABC} L^C, \qquad [R^A, R^B] = \mathrm{i} f^{ABC} R^C, \tag{8}$$

$$[L^A, U] = -T^A U, \qquad [R^A, U] = U T^A, \tag{9}$$

$$[E, U] = U, \qquad [L^A, R^B] = 0. \tag{10}$$

These are operator identities on every fixed-$\mathcal{N}$ sector. The finite Hilbert-space dimension is

$$d_{\mathrm{link}} = \binom{\mathcal{N} + 2N_c N_f - 1}{2N_c N_f - 1}. \tag{11}$$

We audited Eq. (10) for $N_c = 2, 3, 4$ and $\mathcal{N} = 1, 2, 3$. The largest residual was 8.88×10^{-16} [Fig. 2]. This is a direct extension from $U(1)$ to $U(N_c)$, although it is the standard Schwinger/rishon mechanism rather than a new gauge algebra.

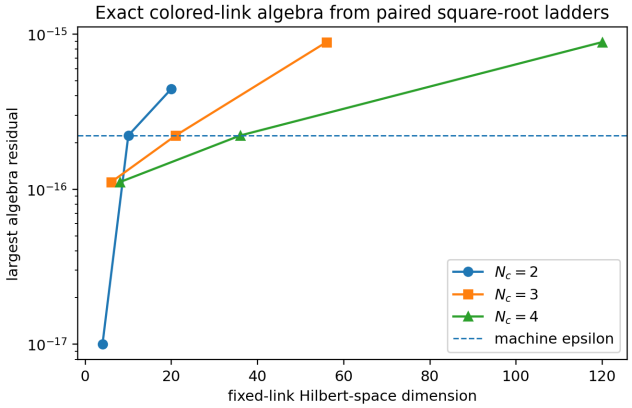

FIG. 2. Largest residual among all color-generator, link-transformation, and Abelian electric commutators. The $U(N_c)$ algebra is exact to floating-point precision for $N_c = 2, 3, 4$.

B. Matter hopping, Wilson loops, and a mobile color

For a link $x \to y$ and fundamental matter ψ_x, the hopping operator

$$H_{xy} = -t \left(\psi^\dagger_x U_{xy} \psi_y + \mathrm{H.c.} \right) \tag{12}$$

commutes with

$$G_x^A = Q_x^A + L_{xy}^A + \sum_{z\to x} R_{zx}^A. \tag{13}$$

A two-site, one-link $SU(2)$ audit has dimension 36 and gives a maximum Gauss commutator exactly equal to zero.

On four consistently oriented links,

$$W_p = \mathrm{Tr}(U_0 U_1 U_2 U_3) \tag{14}$$

also commutes with every local non-Abelian Gauss generator. The residual is zero for both the $N_c = 2$ field space of dimension 256 and the $N_c = 3$ field space of dimension 1296.

We further replaced the scalar plaquette controller by a mobile fundamental color. Its clockwise step is the gauge-covariant Hermitian conjugate of Eq. (12). A complete loop returns the controller to its initial site and generates the matrix holonomy

$$U_3^\dagger U_2^\dagger U_1^\dagger U_0^\dagger \tag{15}$$

inside the returned color block. The 2048-dimensional calculation has zero stepwise Gauss commutator. The fourth-order connected operator agrees with

$$-\frac{t^4}{\Delta^3} U_3^\dagger U_2^\dagger U_1^\dagger U_0^\dagger \tag{16}$$

on its ring-changing support with relative error 1.82×10^{-16}. Thus the autonomous-controller idea extends from an Abelian phase to a non-Abelian matrix holonomy without breaking Gauss's law at intermediate steps.

C. Penalty protection

A two-site $SU(2)$ link with hard-core fundamental matter has a two-dimensional singlet subspace. We added a generic color and link perturbation that does not commute with the six endpoint Gauss generators and evolved

$$H_\Lambda = H_{\mathrm{inv}} + V_{\mathrm{break}} + \Lambda \sum_{x,A} (G_x^A)^2. \tag{17}$$

The maximum dynamical leakage fits

$$P_{\mathrm{leak}}^{\max} = 0.005645\, \Lambda^{-2.00019}, \qquad R^2 = 0.9999983. \tag{18}$$

The expected inverse-square suppression therefore persists for a genuinely noncommuting local gauge algebra [Fig. 3].

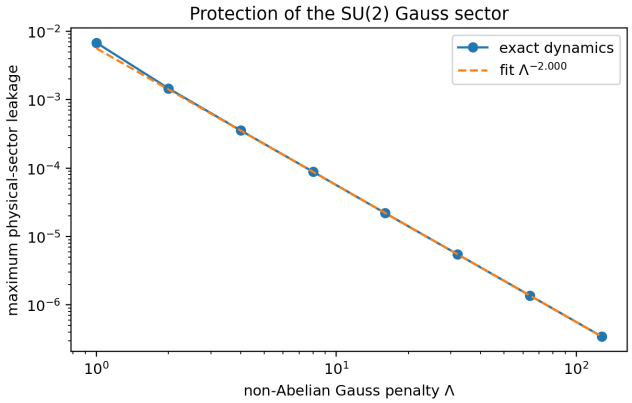

FIG. 3. Non-Abelian Gauss-sector protection under an explicitly gauge-breaking perturbation.

III. A BOSONIC OBSTRUCTION TO PURE $SU(N)$

The link in Eq. (7) naturally carries $U(N_c)$: the non-Abelian subgroup and an additional Abelian electric generator. In quantum-link constructions, a determinant term is commonly used to retain $SU(N_c)$ while breaking the extra link $U(1)$ [2]. For a single bosonic flavor, however,

$$\det U = 0 \tag{19}$$

identically. The columns are built from commuting bosonic creation operators, so the antisymmetrization cancels. This means that merely assigning two colors to the original paired square-root ladders gives an exact $U(2)$ link but does not by itself supply the usual determinant route to a pure $SU(2)$ model.

The obstruction disappears when distinct flavors are available. For

$$U_{\alpha\beta} = \sum_{f=1}^{N_f} a_{\alpha f} b_{\beta f}^\dagger, \tag{20}$$

terms with different flavor labels survive the color antisymmetrization. The audit gives

N_c	N_f	d_{link}	$\|\det U\|_F$ max.	$SU(N_c)$ comm.
2	1	10	0	0
2	2	36	2	0
2	3	78	$\sqrt{12}$	0
3	1	56	0	0
3	2	364	0	0
3	3	1140	6	0

In every nonzero case,

$$[L^A, \det U] = [R^A, \det U] = 0, \qquad [E, \det U] = N_c \det U. \tag{21}$$

Consequently $\det U + \det U^\dagger$ preserves $SU(N_c)$ but not the extra $U(1)$. The minimal bosonic flavor count is $N_f = N_c$ [Fig. 4]. This is the most important correction to the naive claim that a one-flavor bosonic $U(2)$ link can be turned into pure $SU(2)$ without further structure.

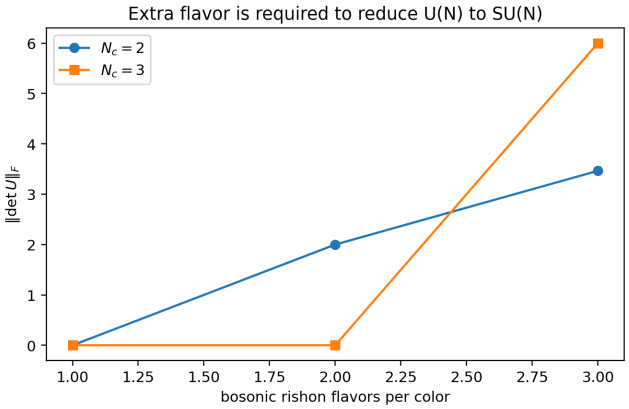

FIG. 4. Frobenius norm of the bosonic determinant operator. At least N_c flavors are required for a nonzero $\det U$ in this construction.

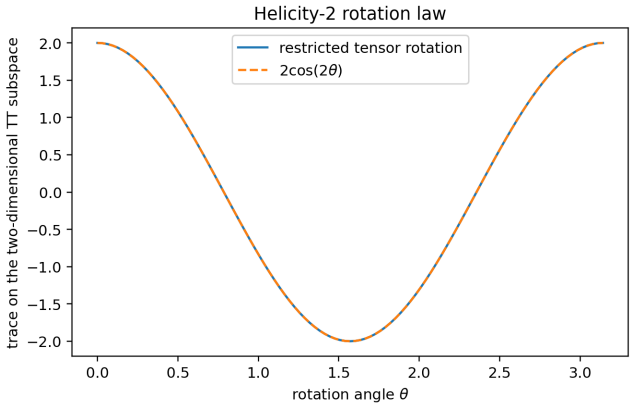

FIG. 5. Character of rotations about the propagation axis. The exact 2θ law identifies the two selected modes as helicity ± 2.

IV. SIX-COMPONENT TRANSVERSE-TRACELESS SECTOR

A. Reduced physical space

Let $h_{ij} = h_{ji}$ and $\pi_{ij} = \pi_{ji}$ be six canonical spatial tensor components. In linearized gravity the canonical constraints and gauge freedom reduce the spatial symmetric tensor to two radiative degrees of freedom [5]. Here we work directly in a lattice TT gauge. Using the real lattice momentum

$$\widehat{k}_i = \frac{2}{a} \sin \frac{a k_i}{2}, \tag{22}$$

the physical components satisfy

$$\widehat{k}_i h_{ij} = 0, \qquad h_{ii} = 0. \tag{23}$$

In an orthonormal six-component basis, let $C(\widehat{\boldsymbol{k}})$ contain the three divergence rows and one trace row. The TT basis Q_{TT} spans $\ker C$, and

$$\Pi_{\mathrm{TT}} = Q_{\mathrm{TT}} Q_{\mathrm{TT}}^T. \tag{24}$$

For every nonzero momentum, $\operatorname{rank} \Pi_{\mathrm{TT}} = 2$.

Across 500 random lattice momenta, the largest numerical residuals were

$$\left\| \Pi_{\mathrm{TT}}^2 - \Pi_{\mathrm{TT}} \right\|_2 = 1.16 \times 10^{-15}, \tag{25}$$

$$\left\| D\Pi_{\mathrm{TT}} \right\|_2 = 1.49 \times 10^{-15}, \tag{26}$$

$$\left\| t\Pi_{\mathrm{TT}} \right\|_2 = 1.02 \times 10^{-15}. \tag{27}$$

Pure longitudinal sources $T_{ij} = \widehat{k}_i v_j + \widehat{k}_j v_i$ and pure trace sources have TT overlap below 5.7×10^{-15}. Thus the source test removes scalar and longitudinal poles exactly within the selected linear sector.

This calculation is a gauge-fixed reduced-phase-space construction. It is stronger than labeling diagonal traceless oscillators "spin 2," but it is not yet a derivation of the full local nonlinear gravitational constraint algebra.

B. Helicity

For a spatial rotation R around the propagation axis, a symmetric tensor transforms as

$$h \mapsto R h R^T. \tag{28}$$

Restricting this representation to the two-dimensional TT subspace gives

$$\operatorname{Tr} R_{\mathrm{TT}}(\theta) = 2 \cos 2\theta, \qquad \det R_{\mathrm{TT}} = 1. \tag{29}$$

The maximum trace error over $0 \le \theta \le \pi$ is 6.66×10^{-16}, and the maximum orthogonality residual is 7.97×10^{-16} [Fig. 5]. The two modes therefore carry helicities ± 2, not merely a pair of traceless labels.

C. Massless scaling and rotational recovery

The reduced free Hamiltonian is

$$H_{\mathrm{TT}} = \frac{1}{2} \sum_{\boldsymbol{k}, \lambda = \pm 2} \left[p_{\boldsymbol{k}\lambda} p_{-\boldsymbol{k}\lambda} + c_T^2 \widehat{k}^2 q_{\boldsymbol{k}\lambda} q_{-\boldsymbol{k}\lambda} \right]. \tag{30}$$

On a periodic box, the smallest nonzero mode gives

$$\Delta_T(L) = 2 c_T \sin \frac{\pi}{L}. \tag{31}$$

Fits over $L = 32$–512 yield

$$\Delta_T(L) \propto L^{-0.999545}, \tag{32}$$

$$\chi_T(L) \propto L^{1.999090}, \tag{33}$$

with $R^2 = 0.99999990$ for both [Fig. 6]. This is a genuine massless $z = 1$ sector by construction, rather than the finite-size saturation previously mistaken for incipient tensor criticality.

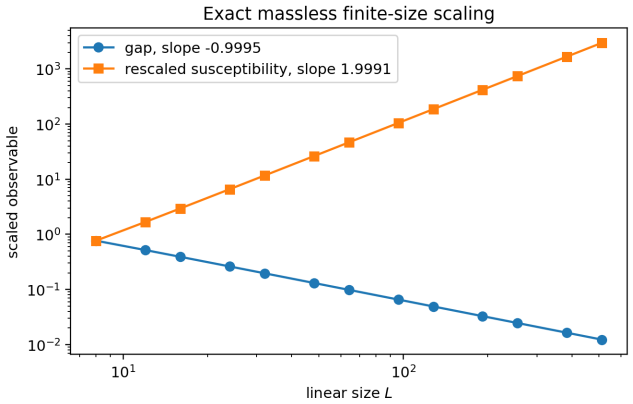

FIG. 6. Finite-size scaling of the exactly massless lattice TT branch. The gap gives $z = 1$ and the free susceptibility gives $2 - \eta = 2$.

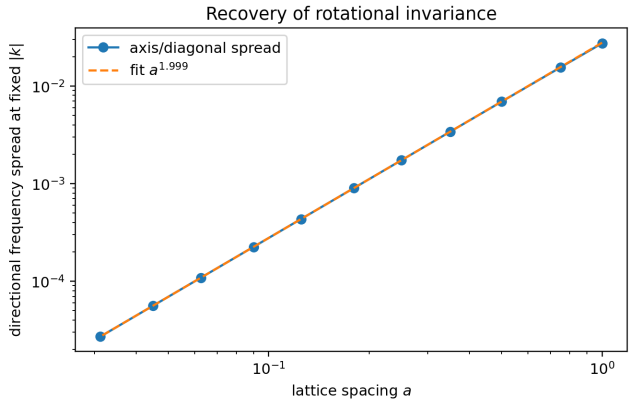

FIG. 7. Cubic directional anisotropy at fixed physical momentum.

At fixed physical $|\boldsymbol{k}|$, the frequency spread between an axis, a face diagonal, and a body diagonal scales as

$$\delta\omega_{\mathrm{cubic}} = 0.02772\, a^{1.99929}, \qquad R^2 = 0.99999995, \quad (34)$$

so rotational invariance is recovered with the expected $O(a^2)$ lattice error [Fig. 7].

D. Constraint protection and the square-root ladder

To test robustness, we mixed all six components with a fixed generic symmetric perturbation of norm 0.15 and separated the non-TT subspace by a penalty Λ. The two lowest modes obey

$$P_{\mathrm{nonTT}} = 0.007032\, \Lambda^{-1.99596}, \quad (35)$$

$$\epsilon_{\mathrm{Ward}} = 0.09919\, \Lambda^{-0.99773}, \quad (36)$$

with $R^2 > 0.9999988$ [Fig. 8]. Amplitudes mix at first order in $1/\Lambda$, while leakage probabilities are second order.

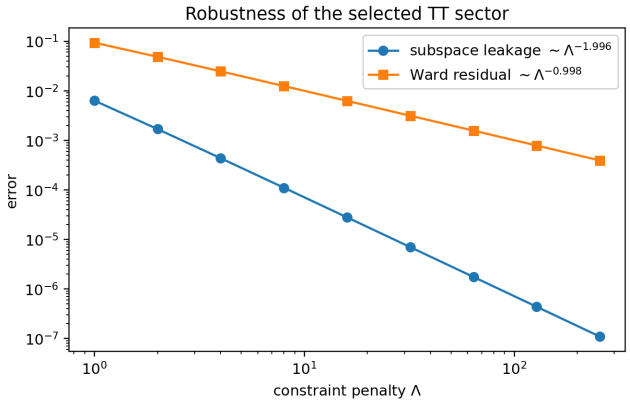

FIG. 8. Suppression of a generic six-component mixing perturbation by the TT-sector penalty.

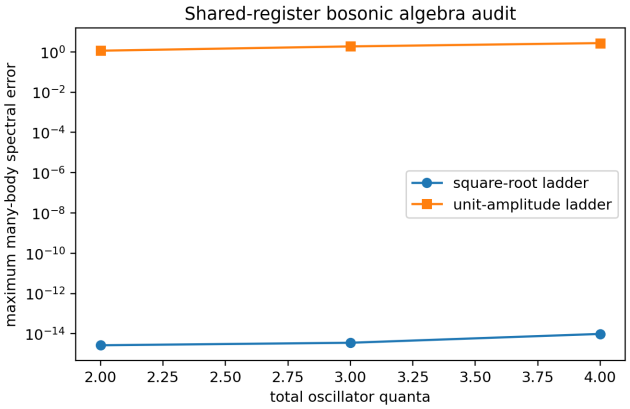

FIG. 9. Multiparticle spectrum of the six-component tensor oscillator.

Finally, we represented all six component modes with the QATNU square-root ladders and tested fixed total occupations of two, three, and four quanta. For a one-particle matrix with eigenfrequencies

$$(0.7, 0.7, 1.8, 1.8, 1.8, 1.8), \quad (37)$$

the exact many-boson spectrum consists of all sums with repetition. Square-root ladders reproduce it with maximum errors 2.7×10^{-15}, 5.3×10^{-15}, and 9.8×10^{-15}. Replacing $\sqrt{n+1}$ by unit amplitude gives errors 1.145, 1.873, and 2.733 [Fig. 9]. The square-root amplitude is therefore load-bearing once repeated occupation occurs.

V. A SELF-CONSISTENT MATTER-COUPLED TENSOR POLE

The earlier comparison of a fixed tensor frequency with a bare two-matter threshold was only a weak-coupling kinematic diagnostic. To make the pole self-consistent,

we use the exactly solvable Friedrichs reduction [6]

$$\begin{aligned} H &= \omega_T(q)|T\rangle\langle T| \\ &+ \int_{E_{\rm th}(q)}^{E_{\rm th}(q)+W} dE\, E|E\rangle\langle E| \\ &+ \int dE\, [v(E)|T\rangle\langle E| + \text{H.c.}]. \end{aligned} \tag{38}$$

The massless lattice tensor branch is

$$\omega_T(q) = 2c_T \sin\frac{q}{2}, \tag{39}$$

and the specified gapped pair threshold is

$$E_{\rm th}(q) = 2\sqrt{\Delta_m^2 + 4v_m^2 \sin^2\frac{q}{4}}. \tag{40}$$

The continuum density is proportional to

$$J_q(E) \propto g^2 (E - E_{\rm th})^{1/2} (E_{\rm th} + W - E)^2, \tag{41}$$

normalized on the finite band. The square-root onset is the generic three-dimensional phase-space behavior at a nondegenerate pair minimum.

Below threshold, the dressed pole solves

$$\begin{aligned} F_q(E) &= E - \omega_T(q) - \Sigma_q(E) = 0, \\ \Sigma_q(E) &= \int dE' \frac{J_q(E')}{E - E'}. \end{aligned} \tag{42}$$

For $E < E_{\rm th}$, $\Sigma_q(E) < 0$ and

$$F_q'(E) = 1 - \Sigma_q'(E) > 1. \tag{43}$$

If the bare level lies below threshold, F_q changes sign exactly once. The model therefore has a unique isolated real pole nonperturbatively in g, with residue

$$Z_T = [1 - \Sigma_q'(E_T)]^{-1} \in (0, 1). \tag{44}$$

For $\Delta_m = 0.76$, $v_m = 0.45$, $c_T = 1.05$, $g = 0.12$, and $W = 2$, the bare branch reaches the continuum at

$$q_{\rm bare} = 1.950043. \tag{45}$$

Dressing preserves an isolated pole through $q \simeq 2.070$ on the numerical grid [Fig. 10]. At $q = 1.2$,

$$\begin{aligned} E_T &= 1.1708133, \qquad Z_T = 0.9825455, \\ E_{\rm th} - E_T &= 0.4395768. \end{aligned} \tag{46}$$

At $q = 2.2$, no isolated pole remains and the continuum peak has FWHM 0.04551; at $q = 2.5$, the FWHM is 0.06427 [Fig. 11].

This is an all-orders statement for the rank-one effective continuum model in Eq. (38). It is not an all-coupling theorem for the complete microscopic matter–tensor Hamiltonian. Closing that stronger claim requires the interacting lattice spectral function and the exact continuum edge of the coupled system.

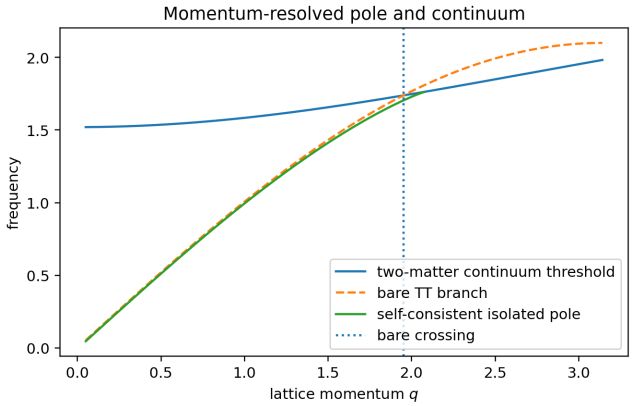

FIG. 10. Bare TT branch, specified two-matter threshold, and the self-consistent isolated pole.

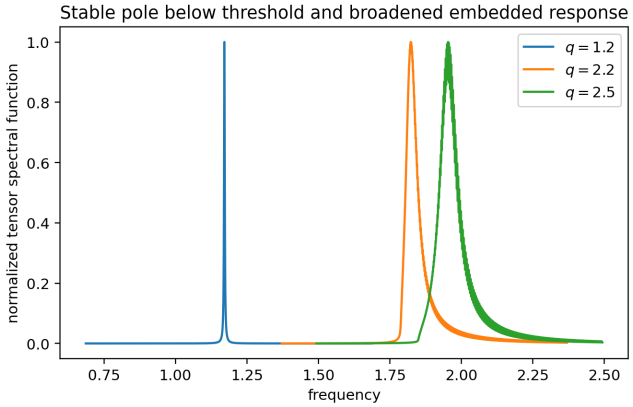

FIG. 11. Normalized spectral functions. The below-threshold pole is resolution limited; after continuum entry the response has a finite width.

VI. WHAT IS ESTABLISHED AND WHAT REMAINS

The calculations establish the following scoped statement:

> A flavored paired-ladder QATNU extension supports exact finite-dimensional $U(N_c)$ quantum links, an explicit route to $SU(N_c)$ after resolving a bosonic determinant obstruction, and a six-component linear tensor sector with exactly two helicity-2, $z = 1$ modes. In a specified gapped continuum reduction, the dressed tensor excitation remains an isolated pole below threshold and broadens after continuum entry.

Several stronger statements remain open:

1. The original one-ladder QATNU Hamiltonian has not been shown to select color, flavor, fixed-rishon, Gauss, or TT constraints dynamically.

2. The $U(N_c)$ construction is the standard rishon quantum-link mechanism. Program-level novelty would come from one native matter–edge Hamiltonian selecting multiple gauge and tensor sectors rather than from the algebra alone.

3. The tensor model is linear and gauge fixed. It does not establish the nonlinear Dirac constraint algebra, universal stress-energy coupling, the equivalence principle, or general relativity.

4. A full microscopic matter-coupled tensor calculation should compute the momentum-resolved retarded Green function and locate the pole relative to the exact interacting continuum.

The next decisive integration is therefore concrete: implement the flavored $U(2) \to SU(2)$ determinant term and the six-component TT register in one local matter–edge simulator, then test whether the low-energy Ward identities and pole separation improve with system size without sending the protecting penalties to infinity.

DATA AND REPRODUCIBILITY

The archive contains the deterministic audit script, full JSON ledger, canonical run log, figures, and checksums. The non-Abelian algebra is audited through $N_c = 4$; the TT tests use 500 random nonzero momenta with fixed seed; all fitted ranges are recorded in the JSON output.

[1] S. Chandrasekharan and U.-J. Wiese, "Quantum Link Models: A Discrete Approach to Gauge Theories," Nucl. Phys. B **492**, 455 (1997), arXiv:hep-lat/9609042.

[2] R. Brower, S. Chandrasekharan, and U.-J. Wiese, "QCD as a Quantum Link Model," arXiv:hep-th/9704106.

[3] U.-J. Wiese, "From Quantum Link Models to D-Theory: A Resource Efficient Framework for the Quantum Simulation and Computation of Gauge Theories," arXiv:2107.09335.

[4] Z.-C. Gu and X.-G. Wen, "Emergence of helicity ±2 modes (gravitons) from qubit models," arXiv:0907.1203.

[5] M. Fierz and W. Pauli, "On relativistic wave equations for particles of arbitrary spin in an electromagnetic field," Proc. Roy. Soc. Lond. A **173**, 211 (1939).

[6] K. O. Friedrichs, "On the perturbation of continuous spectra," Commun. Pure Appl. Math. **1**, 361 (1948).